REPORT DOCUMENTATION PAGE

Public reporting burden for this collection of information is estimated to average 1 hour per response, including the time for reviewing instructions, searching existing data sources, gathering and maintaining the data needed, and completing and reviewing this collection of information. Send comments regarding this burden estimate or any other aspect of this collection of information, including suggestions for reducing this burden to Department of Defense, Washington Headquarters Services, Directorate for Information Operations and Reports (0704-0188), 1215 Jefferson Davis Highway, Suite 1204, Arlington, VA 22202-4302. Respondents should be aware that notwithstanding any other provision of law, no person shall be subject to any penalty for failing to comply with a collection of information if it does not display a currently valid OMB control number. **PLEASE DO NOT RETURN YOUR FORM TO THE ABOVE ADDRESS.**

1. REPORT DATE *(DD-MM-YYYY)*	2. REPORT TYPE	3. DATES COVERED *(From - To)*
17-04-2006	Conference Paper Postprint	2005-2006

4. TITLE AND SUBTITLE	5a. CONTRACT NUMBER
Imaging Sensor & Electronics Assembly for a Responsive Space Experiment	
	5b. GRANT NUMBER
	5c. PROGRAM ELEMENT NUMBER

6. AUTHOR(S)	5d. PROJECT NUMBER
Mark A. Massie, Paul D. LeVan*	
	5e. TASK NUMBER
	5f. WORK UNIT NUMBER

7. PERFORMING ORGANIZATION NAME(S) AND ADDRESS(ES) AND ADDRESS(ES)	8. PERFORMING ORGANIZATION REPORT NUMBER
Nova Sensors 320 Alisal Rd, Suite 104 Solvang, CA 93463	

9. SPONSORING / MONITORING AGENCY NAME(S) AND ADDRESS(ES)	10. SPONSOR/MONITOR'S ACRONYM(S)
*Air Force Research Laboratory Space Vehicles 3550 Aberdeen Ave SE Kirtland AFB, NM 87117-5776	
	11. SPONSOR/MONITOR'S REPORT NUMBER(S)
	AFRL-VS-PS-TP-2006-1018

12. DISTRIBUTION / AVAILABILITY STATEMENT

Approved for public release; distribution is unlimited. (Clearance # VS06-0111)

14. ABSTRACT
An overview of the sensor assembly for an upcoming responsive space demonstration is provided. The "top down" methodology establishing the design baselines, including the sensor array selection, is described in the context of a responsive space payload. The detailed design is then presented. Finally, new data products obtained with the engineering and flight model assemblies for the imager are analyzed and discussed.

15. SUBJECT TERMS
Space Vehicles, Imaging, Space, Visible, Time Delay Integration

16. SECURITY CLASSIFICATION OF:			17. LIMITATION OF ABSTRACT	18. NUMBER OF PAGES	19a. NAME OF RESPONSIBLE PERSON
a. REPORT	**b. ABSTRACT**	**c. THIS PAGE**	Unlimited	14	Paul LeVan
Unclassified	Unclassified	Unclassified			**19b. TELEPHONE NUMBER** *(include area code)* 505-846-9959

Imaging Sensor & Electronics Assembly
for a Responsive Space Experiment

Mark A. Massie
Nova Sensors[1]
Paul D. LeVan
Air Force Research Laboratory[2]

ABSTRACT

An overview of the sensor assembly for an upcoming responsive space demonstration is provided. The "top down" methodology establishing the design baselines, including the sensor array selection, is described in the context of a responsive space payload. The detailed design is then presented. Finally, new data products obtained with the engineering and flight model assemblies for the imager are analyzed and discussed.

Keywords: Imaging, space, visible, time delay integration

Introduction

The optical sensor described herein will collect imagery, in the visible and near-infrared wavelength regions, of ground scenes from a low-earth orbit platform. In the spirit of "responsive space", the optical payload will leverage commercial and existing custom designs for imaging optics and sensor arrays, and tailor (to the greatest extent possible) sensor drive and data acquisition electronics from existing designs in order to demonstrate imaging capability with a minimal design and build phase.

Rapid development of sensor systems for responsive space is challenged both by a compressed timeline and the need to preserve high levels of performance.   This often translates into a combination of high spatial resolution and high sensitivity. In particular, meeting the low noise floor and large dynamic range of commercially-available, visible wavelength sensor arrays is needed to provide adequate scene signal to noise ratios and is found to set limits on analog electronics noise corresponding to less than 1 bit of a 12 bit A-to-D conversion.

Key is the choice of sensor array, and its selection is described in detail. Conventional, non-TDI, line scan sensors provide the largest pixel number and the greater range of pixel pitches from which to choose to optimize a given application, but the downside is that short exposures that preclude image blur in the absence of satellite back scanning capability set stringent limits on the noise floor to achieve even minimal levels of SNR. In a very real sense, a TDI capability is also more forgiving of a higher electronics noise floor that might result in a responsive space scenario, where the schedule for sensor integration may not allow for time-intensive reduction of noise to its ultimate lowest levels. High SNR can be realized by increasing the time-delay integration and the resulting signal level, helping to overcome a slightly-elevated noise floor.

---

[1] 320 Alisal Road, Suite 104, Solvang, CA 93463; mark@novasensors.com
[2] Space Vehicles Directorate, 3550 Aberdeen Ave SE, Kirtland AFB, NM 87117

Design and component selection

Optical

The design of the sensor assembly was dictated in large part by the selection of the telescope – a 20 inch diameter, F/8.1 Ritchey Chrétien (RC Optical Systems, Flagstaff, AZ) modified for space use. The telescope has an approximate 0.75 degree diameter field of view, and when supplemented with a set of refractive corrector optics for field flattening and reduced astigmatism, produces the image quality shown in Figure 1. At a wavelength of 0.75 microns (near the peak of RED-enhanced silicon CCD response), the telescope FOV spans approximately 9000, near-diffraction-limited ("2.4λ/D") pixels, so linear sensor arrays approaching this number of pixels (in length) were deemed of interest for the application.
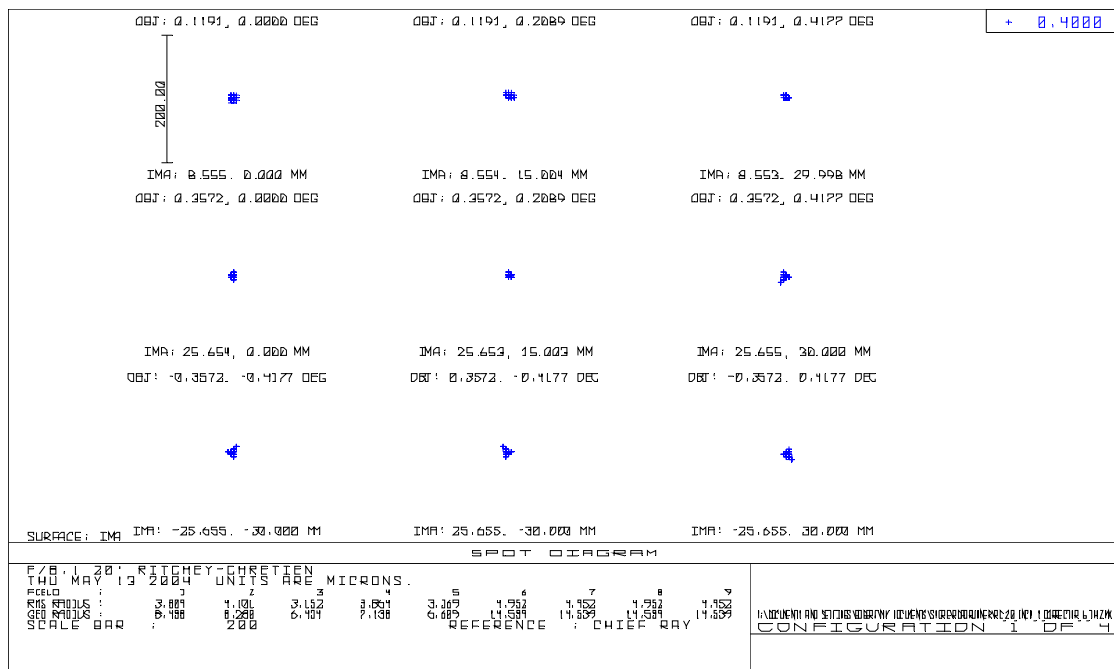

Figure 1 Telescope optical blurs, when set of refractive correction optics is included. The dimensions of the 3x3 array of spots correspond to 0.72 x 0.42 degrees in object space.

With regard to pixel pitch, the 4.1 meter effective focal length of the telescope and a spacecraft altitude of 390 km correspond to 9 cm on the ground for each micron at the telescope focus. Therefore, pixel pitches in the range of 8 to 15 microns correspond to geometrical projections of 0.7 to 1.4 meter, for nadir viewing. The final telescope and sensor array optical properties are summarized in Table 1, below.

Table 1 Fields of view

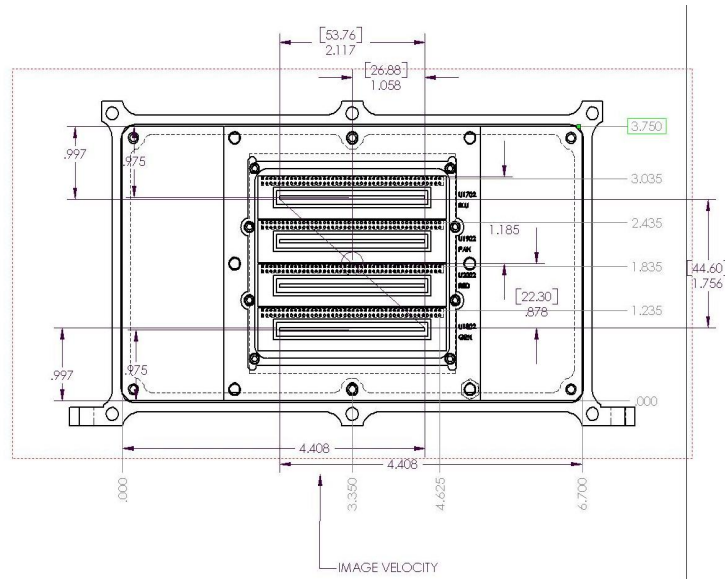| Pixel pitch (um)	Effective telescope focal length (m)	Pixel IFOV (microradians)	Nadir-viewing range (km)	Geometrical FOV at ground (m)
8.75	4.1	2	390	0.8

Figure 2 Geometrical layout of the four sensor arrays in the focal plane.

The Airy disk (with diameter of 2.44 λ (F/#), or approximately 15 microns at a wavelength of 0.75 microns) that contains almost 84% of encircled, point source energy is larger than the 8.75 micron pixel. There are approximately 1.7 pixel samples over the disk diameter, and the extent of one pixel (8.75 microns) encompasses the FWHM of the point spread function (6 microns).

Selection of the Sensor Array

Cross scan field of view (i.e., pixel number) is second to sensitivity in importance. Favorable scene signal to noise ratios are a minimum requirement for the optical sensor. The specific line scan array, and indeed the choice of line scan array over imaging array, was a key selection decision made early, since so much of the remaining optical sensor design relates to it. Selection criteria included (1), preference of line scan array configuration over two-dimensional imaging array for a sensor platform lacking full back-scanning capability and having small (non-zero) levels of pointing drift. As is shown below, exposure times for line scan arrays are typically short (sub millisecond) for minimal blurring of the ground resolution element. Commercially available, two-dimensional imaging arrays tend to reach optimal sensitivities with much longer integration times. (2), preference for a "time-delay and integrate" capability, since the TDI process is essentially noise-free and charge accumulation takes place over the number of selected TDI stages (so a sub-3% well fill could be increased to ~50% after 16 or so stages, for example) and preserves the ground resolution capability of a single TDI integration time.   System noise levels can therefore be held to less exacting standards when TDI capability is employed.   (3), selecting a sensor array having the proper sensitivity for the expected range of scene brightness, optical bandpass, and telescope F/#. (A simple model for the transfer of scene radiance into focal plane array dynamic range is considered in the modeling section, below.) The amount of signal charge integrated over a typical exposure time was compared with the maximum charge capacity of various sensor array types. Also, verification that levels of signal photocurrent exceed the amount of dark current was accomplished over the range of expected sensor array operating temperatures. Finally, signal to noise ratio was then predicted on the basis of fundamental CCD noise mechanisms. For reasons discussed here, a scanning, TDI sensor was chosen (Fairchild CCD 5061, Milpitas, CA) in a 6144 pixel configuration[1].   An image is formed on a line-by-line basis with such a sensor, with the duration of the data collect determining the dimensionality of the resulting image. For example, a square, 6144x6144 pixel image is collected in the time it takes to scan the sensor array 6144 times.

Spectral channels

A four channel sensor was envisioned to utilize the field of view of the telescope as shown in Figure 2, and in analogy to the standard three color scheme ("RGB") but at longer wavelengths and with the addition of a broader, "panchromatic" waveband. The panchromatic waveband would employ most of the useable sensor spectral response, thereby requiring less time-delay integration for a given value of SNR, or allowing higher SNR by using more TDI for fainter conditions of illumination. The set of wavebands should be useful in discriminating vegetation and man-made objects, since the longest waveband emphasizes wavelengths where the reflectance of plants is low. These filter bands are described in Table 2, below. The filter transmission scans are simplistically modeled as shown in Figure 3. The results of combining the filter scans with the detector spectral response are shown in Figure 4.

Table 2 Predicted waveband properties for combined filter transmission and detector spectral response. These can be verified with monochromator scans with the integrated sensor, in the laboratory.

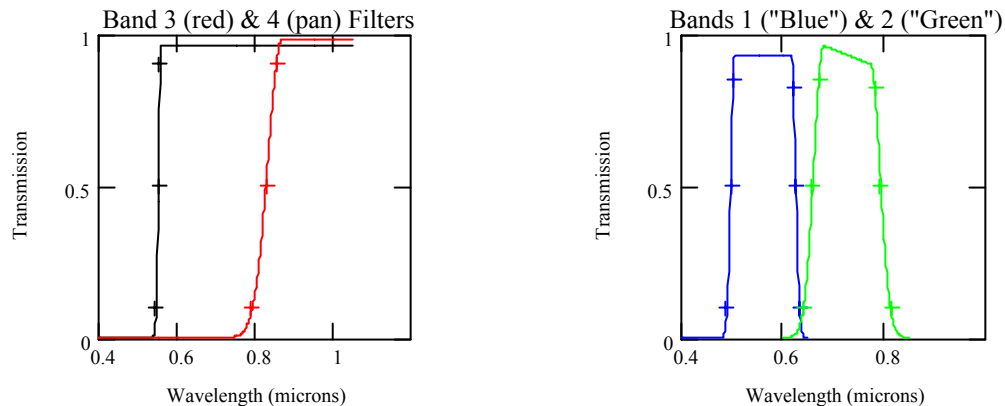| Waveband	Spectral filter wavelengths (um)	Sensor waveband, half-maximum wavelengths (um)	Effective wavelength (um) (combined filter and sensor response)
"RED"	Cut-on, λ=0.83	0.83 & 0.97	0.9
"GRN"	Bandpass, $\lambda\lambda$ = 0.66, 0.79	0.66 & 0.80	0.73
"BLU"	Bandpass, $\lambda\lambda$ = 0.5, 0.63	0.52 & 0.63	0.57
Panchromatic	Cut-on, λ=0.55	0.56 & 0.96	0.77

Figure 3 Simplified models of spectral filter transmission. Note that in the case of the RED and PAN "cut-on" filters, the system waveband cut-offs are determined by the declining detector response near one micron of wavelength.

Alignment among the four sensor arrays is believed to be in the range of +/-1.5 to +/- 5 pixels. Small amounts of image pixel re-grids may therefore be necessary for accurate waveband-to-waveband comparisons of the scene pixels.

Sensor drive & signal processing electronics

The challenges of operating a sophisticated, CCD sensor array incorporating time-delay integration capability include the generation of precise clocking waveforms that have the appropriate timing and amplitudes, providing bias voltages filtered to very low noise levels over a high frequency bandpass, and conditioning and sampling the sensor

outputs prior to A-to-D conversion, which occurs at speeds in excess of 15 million samples per second per sensor output. The noise floor at these high convert speeds corresponds to less than one bit of a 12 bit to-D converter, a very challenging undertaking. An attempt to summarize these requirements are found in the Table 3.

As can be seen in Table 3, the 100 electron noise floor of the sensor array corresponds to ~0.3 mV noise in the analog electronics, up to the input of the A-to-D converter. This level of noise should be maintained over the frequency bandwidth extending up to the 15 MHz A-to-D conversion speed.
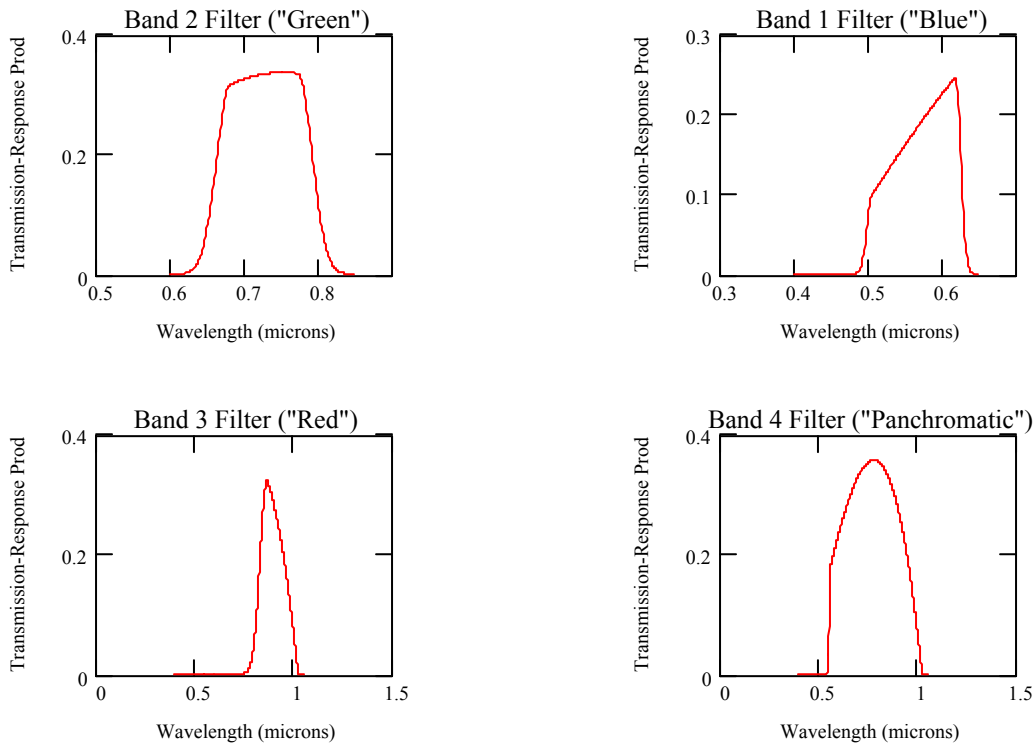

Figure 4 System wavebands, determined with modeled fitting of spectral filter transmission and detector response (see Reference 1 for detector spectral response, for the baseline sensor that includes an anti-reflection window).

Table 3 Sensor array operational parameters, gains, and conversion efficiencies

Sensor array full well (electrons)	Sensor-only read-out noise (electrons)	Sensor array conversion gain (volt/electron)	12 bit, A-to-D converter input range (V)	Sensor assembly conversion gain (counts/electron)	Maximum line scan frequency (lines per sec)	A-to-D convert rate (samples per second, each of 4 sensor outputs)
~450,000	~100	3.3×10^{-6}	1.5	0.0091	9332	$\sim 15 \times 10^6$

Overall sensor electronics architecture
    The four independent 6144 x 128 TDI sensor arrays each require numerous controlling clocks and low-noise bias voltage supplies to operate. A single Field-programmable gate array (FPGA, Xilinx Virtex II XCV300 family device, with approximately 300,000 programmable gates) is used to generate all of the 3.3 volt clock levels as well as

communicate with the spacecraft. A radiation tolerant, programmable, read-only memory (Xilinx XQR18V04 family device) is used to store programming data that is loaded into FPGA memory at system power-on.

A single circuit board (9.5" x 8.0") is used to produce all imager voltage levels. This board also interfaces the four channels of high-speed video data with an on-spacecraft subsystem that performs real-time image processing (the ROPE, or Responsive On-board Processing Experiment).

In addition, a stack of six electronics boards (with each board having dimensions of 6.70" x 3.75" and spaced 0.50" apart) includes the FPGA and PROM combination described above, and is used to perform the rest of the real-time functions of the imager electronics system. These functions include:

- All spacecraft command/control interface processing, with commands received over a uni-directional, RS-422 interface
- All clock level generation and processing, including level shifting to meet the requirements of the sensor arrays. In particular, three-phase clocking waveforms are generated for the sensors' vertical shift registers, and four-phase for the horizontal shift registers.
- All analog video preamplification and conditioning for the sixteen sensor outputs, each of which include correlated double sample (CDS, or perhaps clamp then sample) circuitry, followed by 12-bit A/D conversion.
- System state-of-health monitoring circuits that measure key system temperatures (8 total), voltages (4) and currents (4). The state-of-health data is transmitted over the same data interface bus to the spacecraft as the Panchromatic video data, after being switched into this mode by external command.
- All Channel Link™ serializers (two 21 bit devices for spacecraft-supplied Panchromatic image data and four 28-bit devices for ROPE-supplied RED, GRN, BLU and Panchromatic image data)

As shown in Figure 5, the available sensor line scan frequencies are sufficiently closely spaced to cover the full range of altitudes higher than 362 km. The calculated frequencies are for a telescope boresight that is pointed in the nadir direction over the course of the image collect. At lower altitudes, some blurring of the pixel samples would occur, more so for higher TDI settings.

The sensor assembly is schematically depicted in Figure 6, with its eventual location at the focus of the telescope.
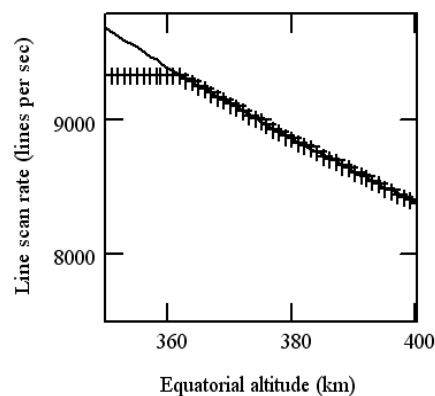

Figure 5 Available line scan frequencies (plus signs) plotted with optimal line scan rates (solid line) as functions of equatorial altitude, for the assumption of continuous nadir pointing of the telescope boresight during an image collect. The deviation in available line scan frequencies at lower altitudes results for the upper limit on system line scan frequency.
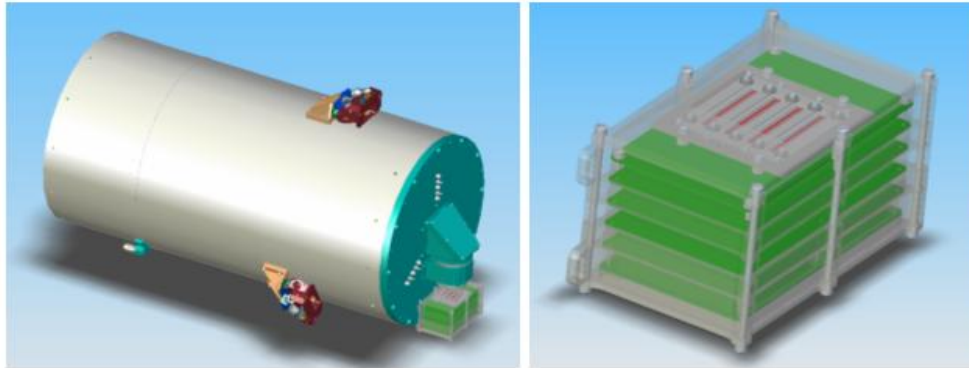
Figure 6 Representation of sensor electronics stack at the telescope focus (left). The four sensor arrays are visible on the uppermost electronics board (right).

Electrical interface requirements

On the sensor side, the four waveband channels each have a sensor array with four output ports, so the requirement for a total of 16 channels of analog electronics and A-to-D conversion was pre-determined. The external interface to which the digital data stream must conform was dictated by the spacecraft as Channel Link™ serializers of two different types (two AeroFlex UT54LVDS217 21-bit input devices to serialize Panchromatic image data for the spacecraft interface, and four National DS90CR285 28-bit input devices to serialize the four colors - RED, GRN, BLU and Panchromatic data - for the on-spacecraft ROPE payload). The overall interface is summarized in Table 4.

Table 4 External interfaces

Interface	Serializer parallel inputs	Number of parallel inputs used (image data only)	Serializer serial outputs (image data only)	Number of sensor A-to-D converters serviced	Serial multiplexing (15 to 30 MHz) of A-to-D outputs	Required number of serializers
Spacecraft	21	12	3	4	X2	2
"ROPE" payload	28	24	4	16	X2	4

As can be seen from Table 4, serializer speeds of 30 MHz allow for overall data transmission rates of 230 million, 12-bit pixels per second – an impressive speed over which 1 LSB noise performance is maintained. The advantage of the adopted approach is that the transmission rate over the serializer interface remains constant at 30 MHz, as different sensor line scan frequencies are selected to match satellite ground scan rates for different altitudes.

State-of-Health (SoH) data

On command, the camera will supply sixteen state-of-health values as well as five additional values relating to imager mode settings. The SoH data is sent by the imager electronics in groups of 16 serializer transfer clock cycles; all SoH data values following the 21 defined values are reported as having constant values as described below and in Table 5. Five additional mode setting words in the second group of 16 are described below:

- "UARTCNT"; the total number of received transmissions across the RS-422 since power-on.
- "PERRCNT"; the total number of transmission parity errors since power-on.
- "PANTDI & REDTDI & GRNTDI & BLUTDI"; programmed TDI code for each color, 3 bits each.
- "LINESYNC"; programmed LINESYNC rate, i.e., sensor line scan rates shown in Figure 5.

- Field-programmable gate array firmware revision number in format M.N, where 8 MSBs represent integer portion (M) ranging 0-255 and 4 LSBs represent fractional portion (N) ranging 0-9.

When a "SoH request" command is received, the imager is first allowed to complete the current group of 6144 sensor pixels, then LSYNC (the clocking waveform for sensor line synchronization status) stays low while the FPGA acquires the SoH data values. The LSYNC waveform then goes high for 32 transfer clocks about 500 us later as the 32 SoH values are clocked out, and returns low again.

If no "SoH terminate" command is received in the meantime, the FPGA immediately repeats the SoH cycle by acquiring new SOH values and clocking them out in the same manner. The LSYNC interval for SoH data is partly dependant on the imager's LSYNC rate for pixel readout. So the interval between LSYNC periods for SoH could be anywhere between 500 us and 700 us, depending on this commanded setting.

If a "SoH terminate" command is received at any time during SOH data output, the current SoH cycle is allowed to complete before the FPGA returns to imager frame outputting, that starts with first four pixels of the four array quadrants, at the time of the appropriate internal frame synchronization signal. In summary, LSYNC is always used as a "data valid" signal for both image and SoH data, and full sensor line scans or full, 32-value SoH data streams are always completed in response to the external commands.

The eleven (11) remaining SoH values in the second group of 16 values are constant and ordered as follows: 0x0000, 0x0111, 0x0222, 0x0333, 0x0444, 0x0555, 0x0666, 0x0777, 0x0888, 0x0999, and 0x0AAA. These may be used in general to verify proper transmission/reception of the SoH values.

Table 5 State-of-Health data

Type	Voltage monitor	Current monitor	Temperature monitor	Status words
Number	4	4	4 internal; 4 external	5
Comments	-5, 3.3, 5, 22V	One for each monitored voltage	External monitors for critical telescope temperatures	Includes line scan frequency & TDI settings

Performance Modeling

We have modeled the level of performance of the sensor assembly in conjunction with the telescope. Our interest is twofold; (1), to gain an understanding of the range in sensor array TDI setting needed for optimal operation of the sensor while in orbit, and (2), to estimate the resulting signal to noise ratios (SNR).

A simple model for the transfer of scene radiance (in watt cm^{-2} SR^{-1} um^{-1}) into focal plane array dynamic range is now described. The optical system throughput, or "A-Ω product", is specified by the optical F/# on the FPA and pixel area. Example values for our F/8.1 and a 8.75 um pixel pitch yield values of A-$\Omega \sim 9 \times 10^{-9}$ cm^2 SR. Spectral bandwidths applicable to the PAN-chromatic channel correspond to $\Delta\lambda$ of 0.4 um (see Table 2). Combining these with the energy of 750 nm photons, a 0.75 transmission loss, and an approximate scene radiance of 0.01 Watt cm^{-2} SR^{-1} um^{-1} (corresponding to a ground reflectivity of 30%, Lambertian reflection & 30 degree solar zenith angle), a representative photon rate (per pixel) of approximately 10^8 photons per sec is the result. Single exposures (without TDI) of approximately 0.1 millisecond over a pixel's dwell time, taken here as the geometrical projection of the pixel on the ground divided by the spacecraft ground speed, result in approximately 10,000 signal photons collected during the dwell time.

In detailed calculations for each of the four sensor wavebands, the signal level is calculated for the "representative" scene defined above over the relevant range of wavelengths. The highly simplified solar spectrum attenuated by the

atmosphere shown in Figure 7 was assumed incident on the ground scene, with additional atmospheric attenuation resulting from the upward pass through the atmosphere of the scene-reflected radiation. In addition to the sensor figures of merit of telescope-pixel "A-omega" product described above, spectral filter transmission and spectral quantum efficiency of the sensor array are also included in the calculations. Noise mechanisms include the readout noise of the combined sensor array and drive electronics (measured under dark conditions), as well as the noise contribution of integrated photocurrent arising from the scene. The level of dark current was found to be negligibly low (< x200 lower than the weakest photocurrent in the "B" waveband channel), even at a higher than typical operating temperature for the sensor array (320 K). The results of the calculations for signal to noise ratio are shown in Table 6.
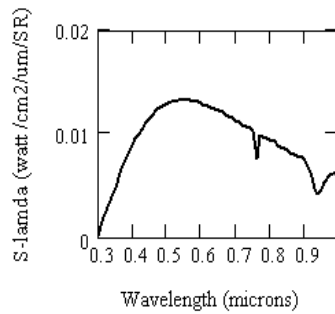

Figure 7 Highly simplified solar spectrum reflected by ground scene and used for performance estimates. As stated in text, the ground is assumed to reflect 30% of the incident solar radiation, isotropically.

Table 6   Preliminary SNR Estimates for Current Spectral Bandpasses

Waveband	50% cut-on/ cut-off wavelength* (um)	Band-averaged Quantum Efficiency**	Filter Transmission (Minimum; averaged over peak)	TDI Setting	Signal electrons (445 ke⁻ full well)	Signal-to-Noise Ratio*** (SNR)
PAN-chromatic	0.56/0.96	0.28	0.95	16	45 ke⁻	200
"BLU"	0.52/0.63	0.19	0.9	64	32 ke⁻	160
"GRN"	0.66/0.80	0.35	0.9	64	63 ke⁻	240
"RED"	0.83/0.97	0.23	0.95	64	50 ke⁻	210

* Weighted by detector spectral response
** From product specification and for sensor delivered with anti-reflection coated window
***@ Line scan frequency of 9332 Hz; corresponds to integration time of 0.1 millisecond (per TDI stage)

    The results of these calculations are encouraging in showing that near-optimal performance (as judged in part by the fraction of charge well filled with signal electrons, Column 7) falls within the allowable range of TDI settings for the sensor array (1 to 128 in powers of two, but excluding 2). This is significant in that it allows trade-offs between longer TDI settings for higher SNR and any degradation in spatial resolution that might result from the longer exposure times. An arbitrarily long TDI setting exacerbates (1), any mismatch in line scan frequency and satellite ground speed for a particular orbital altitude, and (2), susceptibility to spacecraft pointing drift during an image collect.

Methodology for assessing noise performance; preliminary performance assessment
    We can assess the noise floor of the sensor assembly under dark conditions, where the noise contribution associated with integrated photocurrent should not be present. A change in TDI setting (from 1 to 128, for example) confirms that

both photocurrent in the dark condition *and dark current* are sufficiently low to not significantly change the output signal.

Two approaches are pursued to quantify the noise floor. One approach involves only 2, 6144-pixel lines of data. In this approach, signals are differenced on a pixel-by-pixel basis, and the differences divided by √2 to represent the calculation of a standard deviation. This approach is obviously independent of offset variations among pixels, and results in the histogram shown in Figure 8 for the engineering model of the sensor assembly. (The latter incorporates a non-optimal sensor array and excess noise arising from the bias generation amplifiers used only in the engineering models.) The value of the sigma parameter of the Gaussian fitting to this histogram is used to quantify the noise level (in digital counts, standard deviation). This approach was validated with synthetic data for which pixel time samples are random numbers generated with a pre-specified standard deviation. Arbitrary offsets among the pixels were superposed on the random sequences to represent offsets in an actual sensor array. The Gaussian sigma of the resulting histogram was recovered to high accuracy for the synthetic images using the approach outlined above.
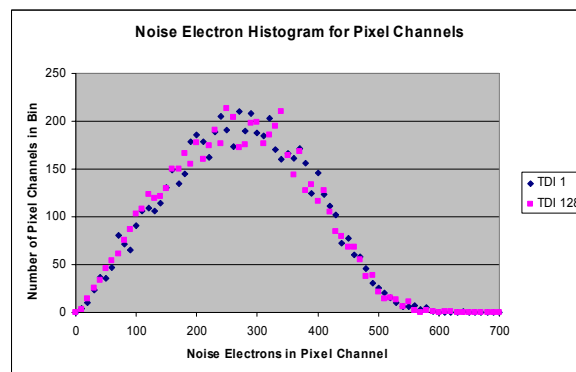

Figure 8 Histogram of 128 image lines, with engineering model sensor in dark laboratory environment. Levels of noise observed under equivalent conditions for the flight sensor assembly exhibit values x2 to x3 lower, which bodes very well for high levels of on-orbit signal to noise.

In the second approach, the standard deviation is calculated for each pixel from many samples. A histogram of the standard deviations reveals the location of the most probable SD, corresponding to the peak of the histogram. The most probable standard deviation was observed to correspond well with the Gaussian sigma found for the "2-line difference" histogram outlined in Approach 1, above. The histogram shows the expected decrease in width as the number of lines (or pixel time samples) increases, but the overall amounts of the decrease have not yet been quantified. As expected, the second approach is more sensitive to longer-term (lower frequency) noise components.

Updated Performance Measurements for Flight Unit

Updated performance measurements have been made to provide additional characterization of the flight version of the imager hardware. These results are included in Figure 9 through Figure 9. Note, these data have been acquired through partial illumination of the 20" telescope aperture, and are thus representative of the combined (telescope and imaging sensor assembly) optical performance. It is believed that electrostatic damage suffered by the "GRN" CCD sensor led to a loss of imaging capability (the sensor array responds to radiation, but spot illumination appears smeared over the array), so data is presented here only for the "PAN", "RED" and "BLU" channels. In general, the dynamic range, SNR and linearity of the individual sensor channels appear to have met the intended operational requirements; the subsystem will continue to be tested in thermal-vacuum and vibration facilities, at the spacecraft level.

For Figure 9, data was taken at 2453 lines/second and at a TDI setting of 128 for all three arrays. The input illumination was provided by a quartz lamp (color temperature ~3400K). The units of illumination are proportional to spectral radiance; i.e., watts/(m^2-sr-um). In Figure 10, the SNR vs. TDI setting was taken at 2453 lines/second for all three channels. The normalized response per color as a function of TDI setting is presented in Figure 11. This indicates that the sensors' TDI function is operating in basically the same manner for all three wavebands
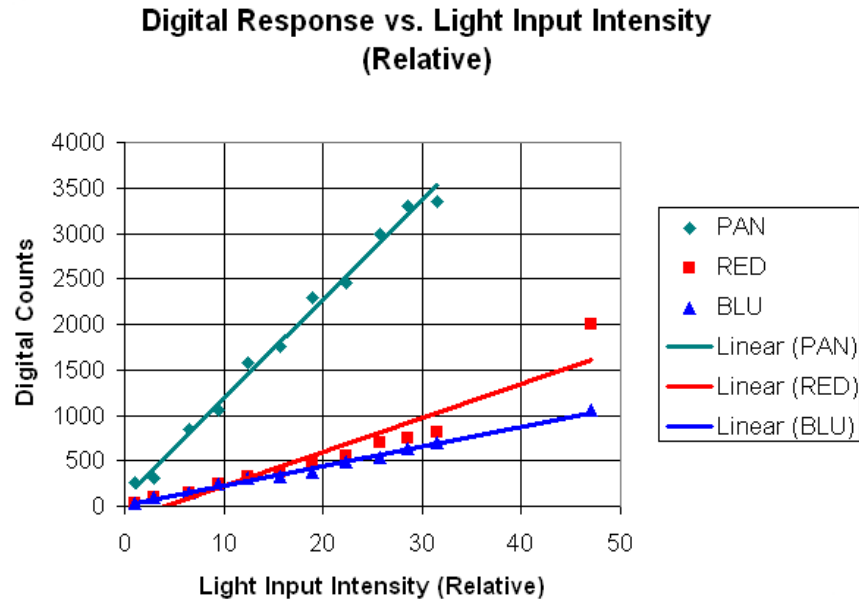
Figure 9 Signal vs. spectral radiance (3400K illumination source) for the PAN, RED and BLU channels with flight spectral filters installed (SAIC data). Common settings for both LSF (2453 lines per sec) and TDI (128) were used. Response is to radiance units (W/m2/SR/um) with an arbitrary geometric scaling factor that is the same for all three wavebands.

We can interpret the key results of Figure 9 in terms of our knowledge of the sensor assembly wavebands, as captured in Tables 2, 3 and 6. Assuming that the overall telescope transmission is roughly equivalent for the four wavebands (an assumption to be verified for the coated Al reflective components; with regard to the three refractive elements, their design was specified to maintain reflection from the two interfaces below 1%, over wavelengths ranging from 0.45 to 1.08 um). The relative responsivities in this case are proportional to $\lambda_{eff} \eta_{eff} \Delta\lambda_{eff}$, with the effective wavelength (λ_{eff}) needed to scale input radiation from watts to photons per second. Calculated effective bandpasses (which, by definition, incorporate the spectral transmission of the filters) are 0.45, 0.12, 0.13, and 0.19 um for the PAN, BLU, GRN, and RED wavebands; values of effective wavelengths (λ_{eff}) and quantum efficiency (η_{eff}) can be found in Tables 2 and 6. The resulting relative responsivities are 7.5/1/2.5/3, for PAN, BLU, GRN, and RED, respectively. For the case of the solar spectrum, the spectral radiance values from Figure 9, combined with these relative responsivity values, yield ratios of 5.6/1/2.1/1.7 for PAN, BLU, GRN, and RED, respectively, which compare favorably with scaling the number of signal electrons in Table 6 to a common TDI setting (180/32/63/50 or 5.6/1/2/1.6).

Alternatively, the ratio of signal responses among the different wavebands should be in proportion to the spectral photon radiance for the source temperature (a 3400 K Quartz lamp) evaluated at the effective wavelength of the waveband, and multiplied by the effective bandpass of the waveband and by the effective quantum efficiency (with values for the effective wavelength and quantum efficiency found in Tables 2 and 6.) Combining these factors with the 3400K spectral photon radiance of 2.3, 1.1, 2.2, and 2.8 x 10^{21} photon/sec/cm^2/um at the effective wavelengths for PAN, BLU, GRN, and RED wavebands, respectively, we predict corresponding signal ratios of 12/1/4.0/4.8 (PAN, BLU, GRN, and RED). These ratios may be compared with those for the solar case, above.

The relative PAN, BLU, and RED responses shown in Figure 9 are therefore seen to be in the correct qualitative sense with the responsivity ratios predicted above (7.5/1/2.5/3, for PAN, BLU, GRN, and RED, respectively), with BLU the

least responsive. The observed, relative RED to BLU response of approximately 1.6 can be compared with the modeled ratio of 3, a difference large enough to cause concern. The observed PAN is x3.4 to x7 stronger that the RED and BLU; this range of ratios seems to be in better agreement with the modeled ratios. The source of any minor discrepancies between observed and modeled responses is currently under investigation, with attention placed on the relative transmission of the refractive optics over the four wavebands, reflectivity differences of the mirror surfaces, or on variations of the published quantum efficiency of the sensor array (with protective cover removed, for this application).

SNR vs. Number of TDI Stages
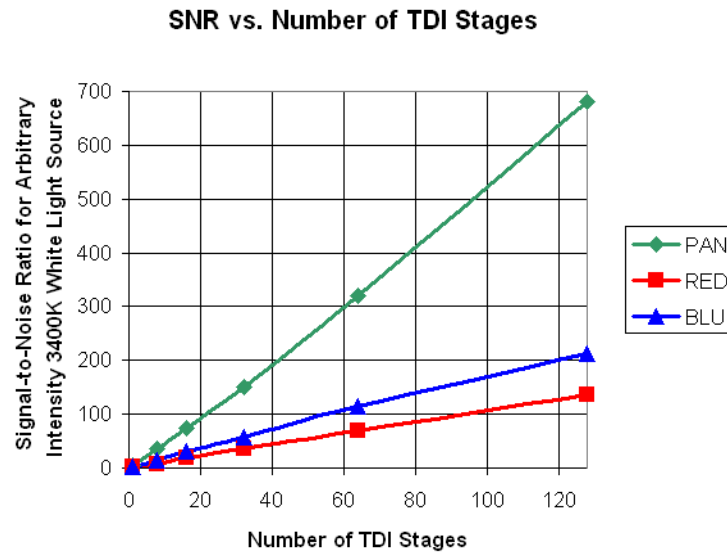
Figure 10 SNR vs. TDI setting for PAN, RED and BLU flight sensor channels (SAIC data), at a common line scan frequency (LSF = 2453 per second).

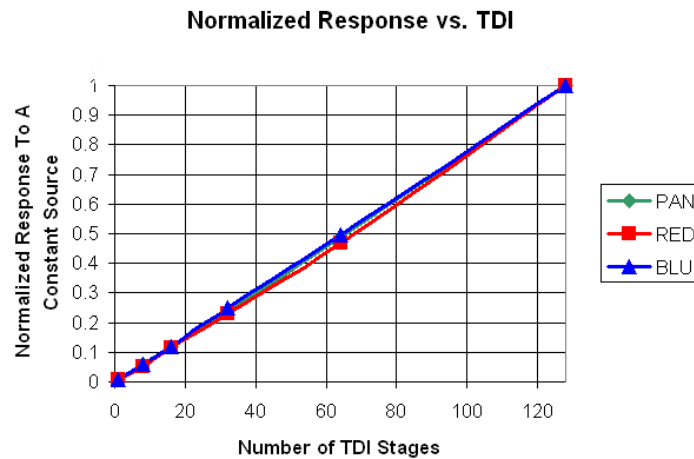## Normalized Response vs. TDI

Figure 11 Normalized response vs. TDI setting for PAN, RED and BLU flight sensor channels (SAIC data).

Figure 12 is a histogram of SNR of the PAN array at an input radiance corresponding to a 30% reflective target and a 20 degree solar illumination angle. To be consistent with previous measurements, this data was also collected using a line rate of 2453 lines/second and a TDI setting of 128, and with a 3400K light source instead of a true solar source.
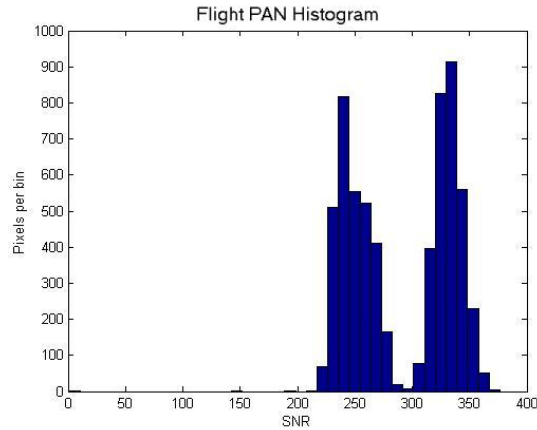
Figure 12 SNR histogram for the 6144 pixels from the fight sensor panchromatic channel, for an input radiance equivalent to a 30% reflective scene and 20° solar illumination angle. The line scan frequency is 2453 per second, using 128 lines of TDI.   The laboratory source temperature is 3400K.   The observed bifurcation is due to offset variations among the four sensor array outputs, which is correctible with a traditional, two-point, non-uniformity correction.

Summary

The baseline design of the imager assembly presented here was originally formulated in Fall 2003, with the exception of the data interfaces to the spacecraft. The initial design has survived the detailed design and build phases of the assembly, and is testimony to the importance of a stable design if rapid development is to be achieved. In particular, levels of noise performance realized with the engineering and flight models of the imager assembly are very promising, and support the notion that signal to noise ratios modeled for the R, G, B, and panchromatic wavebands should be achievable on orbit. Integration with the spacecraft has proceeded in a reasonably smooth fashion.

References

[1]http://www.fairchildimaging.com/main/library/pdf/ccds/CCD5061_021004.pdf

[2]http://www.rcopticalsystems.com/